Journal of Alloys and Compounds 509 (2011) 3025–3031

Contents lists available at ScienceDirect

Journal of Alloys and Compounds

journal homepage: www.elsevier.com/locate/jallcom

Influence of oxygen partial pressure on electrical and optical properties of $Zn_{0.93}Mn_{0.07}O$ thin films

Xue-Yong Li[a,b,c,*], Hong-Jian Li[a,b], Ming Yuan[a], Zhi-Jun Wang[a], Zi-You Zhou[a], Ren-Bo Xu[a]

[a] College of Physics Science and Technology, Central South University, Changsha 410083, China
[b] School of Materials Science and Engineering, Central South University, Changsha 410083, China
[c] School of Sciences, Hunan University of Technology, Zhuzhou 412008, China

ARTICLE INFO

Article history:
Received 9 April 2010
Received in revised form 7 November 2010
Accepted 29 November 2010
Available online 7 December 2010

PACS:
PACS: 71.55.Gs
61.72.Vv
73.40.Lq

Keywords:
Mn-doped ZnO
Microstructure
Electrical properties
Optical properties

ABSTRACT

The $Zn_{1-x}Mn_xO$ ($x = 0.07$) thin films were grown on glass substrates by direct current reactive magnetron cosputtering. The influence of oxygen partial pressure on the structural, electrical and optical properties of the films has been studied. X-ray-diffraction measurement revealed that all the films were single phase and had wurtzite structure with *c*-axis orientation. The experimental results indicated that there was an optimum oxygen partial pressure where the film shows relative stronger texture, better nano-crystallite and lower surface roughness. As the oxygen partial pressure increases, the carrier concentration systematically decreases and photoluminescence peaks related to zinc interstitials gradually diminish. The minimal resistivity of 70.48 Ω cm with the highest Hall mobility of 1.36 $cm^2 V^{-1} s^{-1}$ and the carrier density of 6.52×10^{16} cm^{-3} were obtained when oxygen partial pressure is 0.4. All films exhibit a transmittance higher than 80% in the visible region, while the deposited films showed a lower transmittance when oxygen partial pressure is 0.4. With the increasing of oxygen partial pressure, the peak of near-band-edge emission has firstly a blueshift and then redshift, which shows a similar trend to the band gap in the optical transmittance measurement.

1. Introduction

Diluted magnetic semiconductors (DMS), which combine the two interesting properties: semiconducting and magnetic, are considered as an ideal system for spintronics [1,2]. DMS are formed by partial replacement of the cations of the nonmagnetic semiconductors by magnetic transition-metal ions [3]. As a wide-band-gap II–VI semiconductor, ZnO has been paid much more attention recently as a base material for realizing transparent DMS. On the other hand, ZnO has a band-gap energy in the ultraviolet region (3.37 eV at room temperature) and large exciton binding energy (60 meV) and can be made highly conductive by appropriate doping. Thus its application in optoelectronic devices has been attracted considerably by material scientists [4]. Initially, Dietl et al. [5] have predicted that ZnO would exhibit ferromagnetism at room temperature after doping with 5% Mn ions. After that, there have been a number of reports on the growth of Mn doped ZnO (ZnMnO) films and characterization of their structural, magnetic, optical properties, etc. Most of these studies have been carried out to realize ZnMnO as a DMS. However studies to investigate the other properties such as electrical and optical properties are also necessary.

ZnMnO films have been deposited using different techniques such as molecular beam epitaxy [6], rf magnetron sputtering [7], pulsed laser deposition [8], sol–gel process [9], spray pyrolysis [10], etc. Among these processes used to prepare ZnMnO films, magnetron sputtering is a suitable technique due to the inherent ease with which the deposition parameters can be controlled [11]. The physical properties of ZnMnO films prepared by magnetron sputtering are generally dependent on deposition parameters including the oxygen partial pressure, sputtering power, substrate temperature, etc. The physical properties of the films relative to the substrate temperature in deposition have been investigated widely. However, the effect of oxygen partial pressure on physical properties of thin films has not been studied in detail yet. In this work, Mn doped ZnO films have been deposited by direct current (dc) magnetron sputtering and the influence of oxygen partial pressure on the structural, surface morphological, electrical and optical properties of Mn doped ZnO thin films has been investigated.

2. Experimental details

Mn-doped ZnO thin films were grown on glass by dc magnetron cosputtering. The 99.99% pure Zn metallic target, along with some smaller ruleless Mn slices laid on Zn disk, was used as the sputtering target. The Mn-doped concentrations were

* Corresponding author at: College of Physics Science and Technology, Central South University, Lushanlu 8#, Changsha 410083, Hunan, China.
Tel.: +86 731 88830863; fax: +86 731 88830857.
E-mail addresses: lixueyong@163.com (X.-Y. Li), lihj398@yahoo.com.cn (H.-J. Li).

0925-8388/$ – see front matter © 2010 Elsevier B.V. All rights reserved.
doi:10.1016/j.jallcom.2010.11.191

controlled by changing the number of Mn slices. The base pressure in the chamber was 5×10^{-4} Pa and the distance between the target and substrate was set at 70 mm. The glass substrates were first cleaned in propanone and ethyl alcohol solutions in an ultrasonic bath for 15–20 min, rinsed in deionized water and finally dried in high purity N_2 gas stream. High purity (99.999%) Ar and O_2 gas was introduced into the chamber and was metered by mass flow controllers for a total flow rate fixed at 15 sccm. In order to clean the target surface, a pre-sputtering process was employed for 10 min in Ar gas before depositing films. During deposition, the substrate was rotated with a frequency of 60 rpm, the substrate temperature, dc power, and sputtering pressure were kept at 200 °C, 100 W, and 1.0 Pa, respectively. Oxygen partial pressure was defined as R ($R = P_{O2}/(P_{O2} + P_{Ar})$) and R was varied from 0.3 to 0.5. All the films were deposited for 60 min, the resulting thickness of all the films is about 500 nm.

A conventional stylus surface roughness detector (Alpha-step 200) was used to measure the thickness of thin films. The composition and chemical bonding of the films were determined using X-ray photoelectron spectrometer (XPS: VG Scientific, ESCALAB MARK II). The film surface was sputtered by an Argon ion gun operated at 2.5 keV (etching rate 2 nm min^{-1}) for 10 min and the analysis area was 200 μm × 200 μm. The pass energy of 50 eV and the X-ray power of 100 W were employed, respectively. The XPS spectra were recorded using monochromatic AlKα excitation (1486.6 eV), and the reflections in the XPS spectra were calibrated by taking the carbon C 1s peak (284.6 eV) as a reference. During the measurements, working pressure was kept at 5×10^{-7} Pa. The structure and crystalline quality of the samples were detected with X-ray diffraction (XRD) using Cu-Kα radiation (λ = 0.1541 nm) of a SIEMENS D-500 diffractometer operating at 40 kV, 30 mA for angles between $2\theta = 10^\circ$ and 70° in 0.05° steps. The surface morphology was investigated using atomic force microscopy (AFM, SOLVER P47) in the tapping mode. Silicon nitride tips with a tip curvature radius smaller than 7 nm were used. The average height was determined by analysing the topographic data in area of 1 μm × 1 μm. The film resistivity was determined by a simple dc four-point probe system (SZT-90). The carrier concentration and Hall mobility were measured by a Hall measurement system (HMS 3000) with the Van der Pauw method. Optical transmittance measurements were carried out using a UV–vis spectrophotometer (TU-1800PC) in the wavelength range from 200 to 1100 nm. The photoluminescence (PL) spectrums within the wavelength range 330–600 nm were obtained under 325 nm line of Xe laser excitation using a fluorescence spectrophotometer (F-2500). All measurements were performed at room temperature.

3. Results and discussion

3.1. Compositional analysis and structural properties

The visual appearance of all ZnMnO films grown in the oxygen partial pressure range from $R = 0.3$ to $R = 0.5$ strongly adherent to the substrate surface with a straw yellow color in appearance. The composition and chemical bond configuration of the elements present in the films were estimated using XPS measurements. Fig. 1 shows the XPS spectra of the experimental films deposited at $R = 0.4$. In Fig. 1(a), two peaks at the binding energies 640.7 eV and 652.3 eV are corresponded, respectively to the Mn $2p_{3/2}$ and Mn $2p_{1/2}$. No XPS signals from metallic Mn (637.7 eV) and Mn^{4+} ions (642.4 eV) were detected. These results indicate that the doped Mn ions are in divalent states and Mn ions have been doped into the interior of the nanostructure owing to these two weak XPS peaks. Fig. 1(b) presents the binding energy of Zn $2p_{3/2}$ is 1021.7 eV with a narrow linewidth of 1.86 eV, implying only a single component of Zn^{2+} ions. The broad and asymmetric of O 1s peak, implying the presence of a multi-component of O, can be disconvoluted by the best fitting with Gaussian function into two peaks as shown in Fig. 1(c). The left centered at 530.1 eV can be attributed to O^{2-} ions in Zn–O and Mn–O bonds, the right centered at 532. 0 eV can be allocated to the loosely bound oxygen chemisorbed on the surface and/or grain boundary of polycrystalline film [12]. Form XPS measurements, the Mn concentration in the films was estimated to be 7.39%, 7.32%, 7.26%, 7.21% and 7.11% as the deposition oxygen partial pressure was 0.3, 0.35, 0.4, 0.45, 0.5, respectively. Therefore, the atom fraction of Mn doped in film is approximately 7% for all samples ($Zn_{0.93}Mn_{0.07}O$).

XRD measurements were performed in order to examine the variation of structural properties with varying oxygen partial pressure. Fig. 2(a) shows the XRD patterns of $Zn_{0.93}Mn_{0.07}O$ thin films deposited at different oxygen partial pressures. This is a broad peak

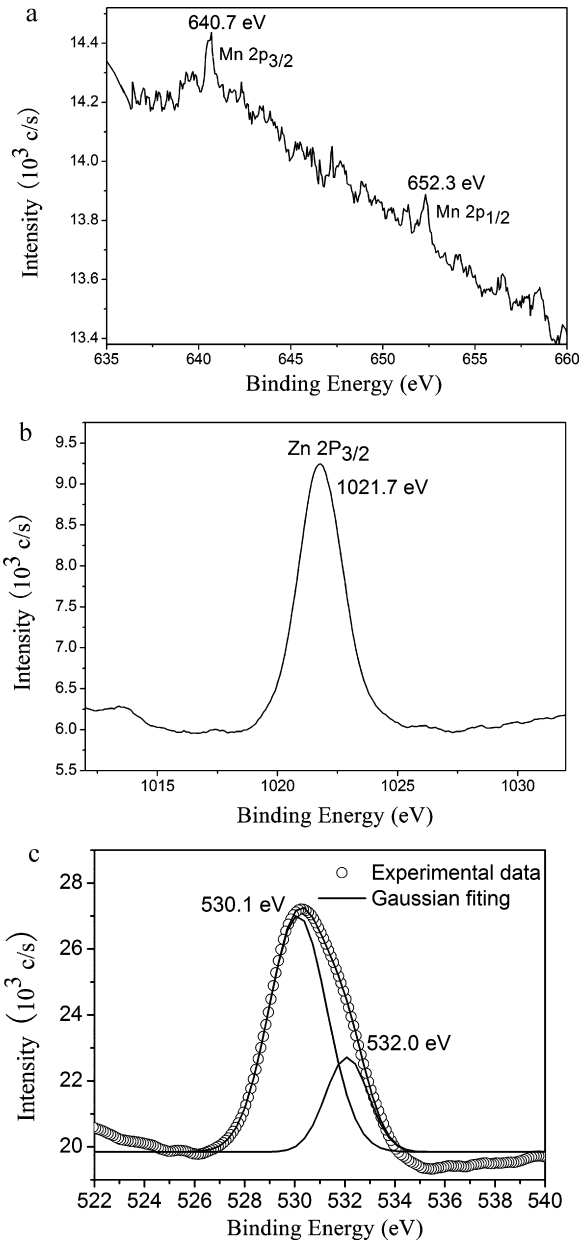

Fig. 1. XPS spectra of $Zn_{0.93}Mn_{0.07}O$ films ($R = 0.4$). (a) Mn $2p_{3/2}$ and Mn $2p_{1/2}$ region; (b) Zn $2p_{3/2}$ region; (c) O 1s core level region.

around 20° for XRD patterns for ZnMnO films, it shows the amorphous nature of the glass substrate. All the films showed only a strong peak at 2θ near 34° in the diffraction angle (2θ) region from 10° to 70°, which were identified the (0 0 2) peak of hexagonal ZnO. In addition, another small peak at 2θ near 32° that correspond to the (1 0 0) orientation of ZnO was also presented. Here during deposition of ZnO, Mn atoms may act as obstacle for the growth of ZnO along (0 0 2). In this study, Mn doped ZnO does not induce distinguishable effects in X-ray spectra and other new phases (within the XRD detectable limit), which might be attributed to a little amount of Mn in the matrix of ZnO. The results indicate that Mn ions tend to substitute for Zn sites without changing the crystal structure of ZnO (wurtzite structure), and the *c*-axis is a strong preferred orientation. It is found that the intensity of (0 0 2) orientation of the films increases with the oxygen partial pressure up to 0.4 and decreases with further increase of oxygen partial pressure. At low oxygen partial pressures, the oxygen deficiency

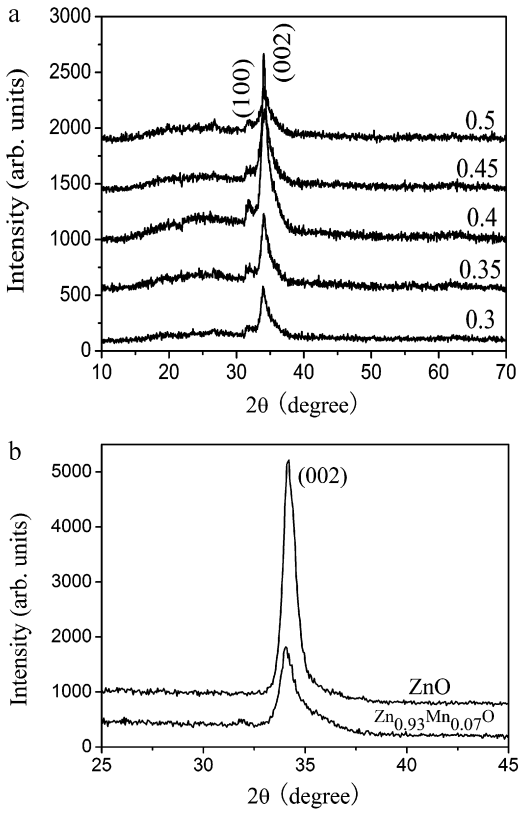

Fig. 2. XRD patterns of ZnMnO and ZnO films. (a) XRD patterns of $Zn_{0.93}Mn_{0.07}O$ films deposited at different oxygen partial pressures; (b) XRD patterns of ZnO and $Zn_{0.93}Mn_{0.07}O$ films deposited at $R = 0.4$.

leads to the incomplete reaction of O and zinc atoms, which will weaken the preferred (0 0 2) orientation. For intermediate oxygen partial pressures, the films have a maximum volume fraction of the crystallized phase. Whereas, with the further increasing of oxygen content, the resputtering effect by neutral oxygen becomes greater. This resputtering effect of O atoms is considered to hinder grain growth and cause film amorphization. In addition, the excess oxygen causes a surface oxidation of the target, which usually reduces the sputtering yield and thus reduces the orientation too. Compared to the undoped ZnO, the XRD 2θ peak of $Zn_{0.93}Mn_{0.07}O$ (0 0 2) is weak and broad [Fig. 2(b)]. This is presumable due to lattice disorder and strain induced by Mn^{2+} ions substitution [8,13]. The characteristic parameters given by XRD from the (0 0 2) plane can used to characterize the structural feature of these films, all the calculated results are summarized in Table 1.

Information concerning position of XRD peaks (2θ) as a function of oxygen partial pressure is given in Table 1. The position of the (0 0 2) peaks shifts to the higher angles with the increasing of oxygen partial pressure up to 0.4 and then shifts to the lower angles with further increasing of oxygen partial pressure. The diffraction peak position of 2θ shifts towards lower angle compared to bulk ZnO value (34.43°) for all samples, it can be attributed to the residual stress in the films [14]. Based on the Bragg formula, the lattice parameter of c has been estimated to be 0.52482–0.52858 nm, that is larger than the value of 0.52069 nm for bulk ZnO [15]. This is presumably results from the substitution of Mn ions with a large ionic radius of 0.083 nm for Zn (0.074 nm) sites [16]. Since the ionic radius of Zn^{2+} (0.074 nm) is smaller than that of Mn^{2+} (0.083 nm) and larger than that of Mn^{3+} (0.065 nm) and Mn^{4+} (0.054 nm), the larger c-axis lattice constant indicated that the divalent Mn^{2+} ions substituted for Zn^{2+} ions in ZnO crystal lattice [16]. The lattice constant c is used to estimate the strain (ε) in the films along c-axis given by the following equation [17]: $\varepsilon = [(c_{film} - c_{bulk})/c_{bulk}]$, where c_{bulk} is the unstrained lattice parameter measured from bulk ZnO and the value of c_{bulk} is 0.52069 nm [15]. The calculated results are also shown in Table 1. The thermal strain introduced by the different linear thermal expansion coefficients α of film ($\alpha_{ZnO} = 4 \times 10^{-6}\,K^{-1}$) and glass substrate ($\alpha_{glass} = 9 \times 10^{-6}\,K^{-1}$) is significantly smaller than the measured strain. It shows that the measured film stress is mainly caused by the growth process itself rather than thermal origin. The lattice constant 'c' of $Zn_{0.93}Mn_{0.07}O$ films is larger than the bulk ZnO. According to the results in Table 1, the strain in the films is positive, suggesting that the films contain residual compressive stress. From above discussions, it suggests that the stress is generated during deposition due to the substitutions of Mn ions and other intrinsic defects like vacancies and interstitials of Zn and O. Furthermore, bombardment of growing films with ions can lead to significant stress levels. It has been reported in the case of ZnO films that energetic particles (Ar^+ at low oxygen content and negative oxygen ions at high oxygen content) have sufficient energies to bombard the growing film and cause implantation or displacement of surface atoms deeper into the film, resulting in compressive strain [18]. Due to the improvement of the homogeneity and the stoichiometry of the films with the increasing oxygen partial pressure in a suitable range, the relaxation of $Zn_{0.93}Mn_{0.07}O$ films is observed. The film prepared at oxygen content of 0.4 seems to have the smallest stress because its c value is most close to the standard value. Higher or lower oxygen content would lead to increasing of the mechanical stress.

The full width at half-maximum (FWHM) can be used to estimate the crystallite size along c-axis, based on the XRD results, the average size D of the crystalline grains along the c-axis can be evaluated using the Debye–Scherrer formula:

$$D = \frac{0.9\lambda}{B\cos\theta} \quad (1)$$

where λ is the X-ray wavelength(0.1541 nm), θ is the Bragg angle, and B is the FWHM of the (0 0 2) diffraction peak. The variation of crystallite size with the increases of oxygen partial pressure is shown in Table 1. As can be seen from Table 1, the grain size of the film is about 7–13 nm. The strongest reflection from c-plane is observed when R is 0.4, while the grain size reaches its maximum due to its smallest FWHM. The results above indicate that there has an optimum oxygen partial pressure where the film shows relative stronger texture and better nano-crystallite. In addition, the oxygen content in this work gas has great effect on the surface morphology of films. Fig. 3 illustrates the AFM imaging of the surfaces of $Zn_{0.93}Mn_{0.07}O$ films deposited at oxygen partial pressure. In Fig. 3(a), the surface morphology of the thin films deposited at low oxygen partial pressure shows a coarse surface with small grains. With increasing oxygen partial pressure, the grain size becomes larger and the film has a smoother surface due to the balance of the reaction effect and bombardment effect. In addition, as has been studied by the XRD analyses, the compressive stress is released by increase of oxygen partial pressure. More or less, it is related to the enhanced mobility of atoms to lower energy sites on the sur-

Table 1
Parameters of XRD patterns (2θ), FWHM, c, strain (ε) and crystallite size (D) of $Zn_{0.93}Mn_{0.07}O$ films deposited at different oxygen partial pressures.

R	2θ (°)	FWHM (°)	c (nm)	ε ($\times 10^{-3}$)	D (nm)
0.3	33.9	0.93	0.52858	15.153	8.93
0.35	34.05	0.84	0.52632	10.813	9.89
0.4	34.15	0.62	0.52482	7.932	13.41
0.45	34.10	1.12	0.52556	9.353	7.42
0.5	34.02	1.15	0.52676	11.658	7.23

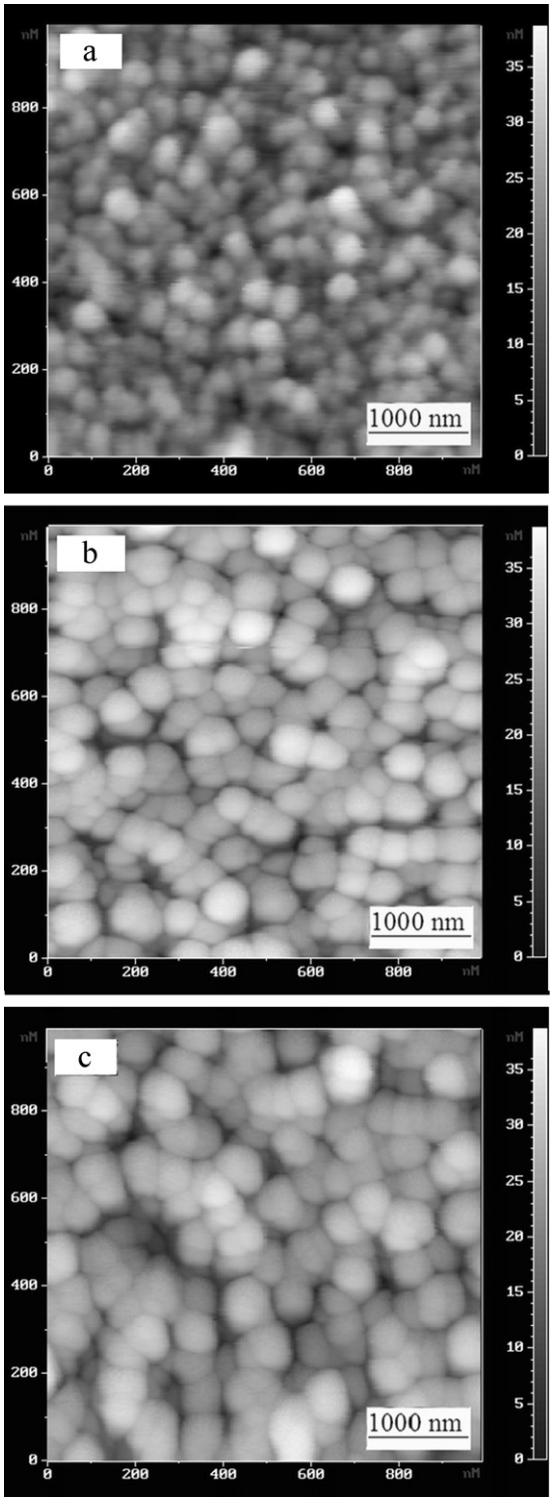

Fig. 3. AFM images of the surfaces of $Zn_{0.93}Mn_{0.07}O$ films deposited at different oxygen partial pressures. (a) $R = 0.3$; (b) $R = 0.4$; (c) $R = 0.5$.

face as a result of the improved crystalline structure of the films. As can be seen from Fig. 3(b), the $Zn_{0.93}Mn_{0.07}O$ film prepared at optimum oxygen partial pressure of R is 0.4 has a compact, dense and uniform structure, with the crystallite dimension normal to the c-axis of about 80 nm and the average surface roughness is 5.122 nm. However, when R is increased up to O_2 overpressure, surface of thin films is locally agglomerated with an incompact structure. It might be due to re-sputtering of high-energy neutral oxygen atoms [19].

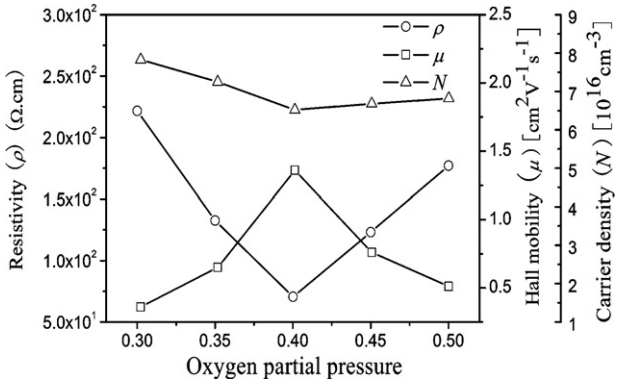

Fig. 4. Resistivity (ρ), Hall mobility (μ) and carrier concentration (N) of $Zn_{0.93}Mn_{0.07}O$ films deposited at different oxygen partial pressures.

3.2. Electrical properties

The effect of oxygen partial pressure on the electrical properties (resistivity ρ, Hall mobility μ and carrier concentration N) of $Zn_{0.93}Mn_{0.07}O$ films is shown in Fig. 4.

At room temperature, the n-type carrier concentration is of the order of $10^{16}\,cm^{-3}$ for all samples. The minimal resistivity of $70.48\,\Omega\,cm$ with the highest Hall mobility of $1.36\,cm^2\,V^{-1}\,s^{-1}$ and the carrier density of $6.52\times10^{16}\,cm^{-3}$ were obtained when oxygen partial pressure is 0.4. As R is in the region of 0.3–0.4, resistivity decreases with oxygen partial pressure increasing. The decrease can be ascribed to the improvement of crystallization that can enhance the mobility of the carriers while the carrier concentration fluctuating mildly. A further increasing oxygen partial pressure will favor the films approach stoichiometry, resulting in no increase or even a decrease in conductivity.

Since Mn^{2+} is an isovalent impurity in the ZnO matrix, no change in the carrier concentration can be expected. The conduction electrons in ZnO films are supplied from donor sites associated with oxygen vacancies or Zn interstitial atoms. The donor could be either an impurity or an intrinsic defect, since that both zinc interstitials and oxygen vacancies can act as shallow donors. The strong dependence of resistivity on oxygen partial pressure implies that oxygen vacancies play a more important role in the conductivity of the films. Lower oxygen partial pressure will lead to more oxygen vacancies and release more free electrons, resulting in a higher carrier concentration. As shown in Fig. 4, the carrier concentration is mildly decreased with increasing R up to 0.4. The decrease of carrier concentration is originated from the decrease of Zn interstitials and oxygen vacancies acting as donors with increasing in oxygen partial pressure. Above R is 0.4, carrier concentration is very slightly increased with increasing R, and it might be attributed to the increase of grain boundaries. The electron mobility depends on several scattering mechanisms such as grain boundary and ionized impurity scattering. Oxygen vacancies may be the source of the dominant impurity scattering in the low oxygen partial pressure, but the grain boundary scattering is the dominant impurity scattering at high oxygen content. As presented in Fig. 4, the higher impurity scattering results in the lower Hall mobility. With the increasing oxygen partial pressure in a suitable range, which reduces the structural defects and improves crystalline structure of the films, thus a enhancement of the mobility is observed. Further increase in oxygen partial pressure reduces the Hall mobility, possibly as a result of electron scattering by the defects/ionized impurities.

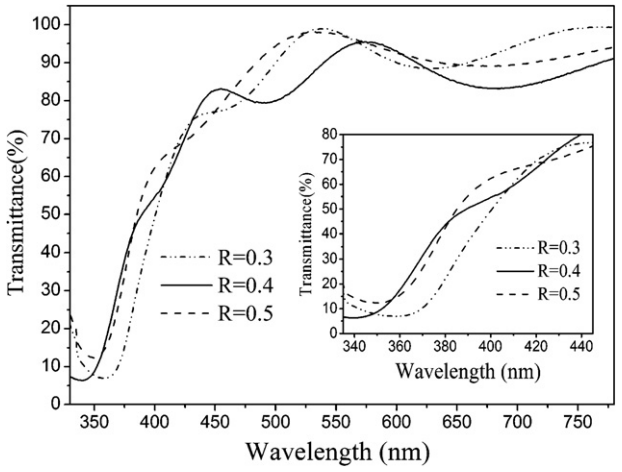

Fig. 5. Room-temperature transmittance spectra of $Zn_{0.93}Mn_{0.07}O$ films deposited at different oxygen partial pressures (the inset shows the enlarged transmittance spectra between 335 and 435 nm).

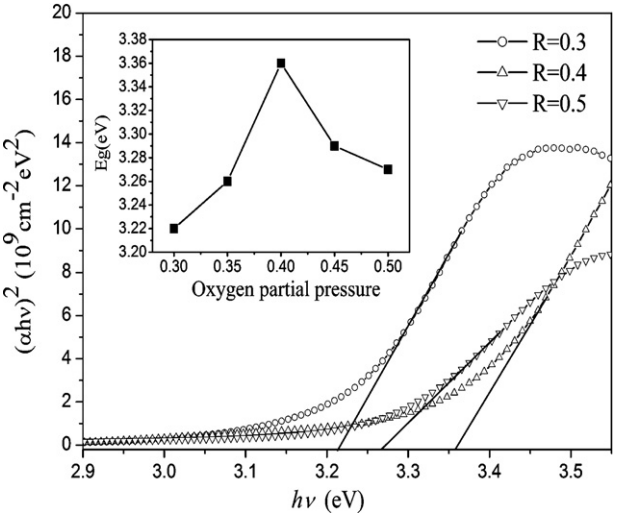

Fig. 6. The $(\alpha h\nu)^2$ versus $h\nu$ curves for the optical band gap determination of $Zn_{0.93}Mn_{0.07}O$ films deposited at different oxygen partial pressures (the inset is the optical band gap of $Zn_{0.93}Mn_{0.07}O$ films deposited at various oxygen partial pressure).

3.3. Optical properties

3.3.1. Transmittance

The room temperature transmittance of $Zn_{0.93}Mn_{0.07}O$ films deposited at different oxygen partial pressures is shown in Fig. 5. Obvious interference phenomenon can be observed in every spectrum, indicating a smooth and homogeneous surface of the films. With increasing of R from 0.3 to 0.35, 0.4, 0.45, and 0.5, the average transmittances of $Zn_{0.93}Mn_{0.07}O$ films are 85.9%, 88.2%, 80.5%, 84.9% and 86.7% in their visible regions, respectively. The average transmittances (without glass substrate deduction) in the visible regions within the wavelength from 380 to 780 nm are more than 80% for all specimens. However, the films prepared show lower optical transmittance when R is 0.4. Therefore, the absorption is the largest when R is 0.4 even an improvement of crystalline structure and the stoichiometry of the films. That indicates Mn atoms might act as obstacle for the optical transmittance of $Zn_{1-x}Mn_xO$ films. Compared with Fig. 4, the higher the carrier density, the better transmittance in the visible region. The reason for it might be attributed to the presence of Zn interstitial atoms in the samples deposited at lower or higher oxygen partial pressure that makes it somewhat translucent as compared to other samples and hence decreases its refractive index. Since the refractive index of the zinc metal is 1.002050 [20], hence their presence in the ZnMnO films decreases the overall refractive index of the films and a higher optical transmittance is observed. When R is 0.4, the reaction effect and bombardment effect turn to be balance, and therefore Zn interstitials in the films become negligible and exhibit a lower optical transmittance.

As seen in Fig. 5, a sharp absorption edge below 400 nm is observed in all the films due to the onset of fundamental absorption of ZnO. With increasing oxygen partial pressure within a suitable range, the optical absorption edge of $Zn_{0.93}Mn_{0.07}O$ films has a significant blueshift to the region of higher photon energy. The optical absorption coefficient (α) is evaluated from the transmission spectra using the following relation:

$$T = A\exp(-\alpha d) \quad (2)$$

where T is the transmittance of the films, A is the constant, and d is the film thickness. For ZnO with direct allowed transition band structure, the optical band gap of the films is given by [21]:

$$\alpha h\nu = C(h\nu - E_g)^{1/2} \quad (3)$$

where $h\nu$ is the photon energy, E_g is the optical band gap, and C is a constant for a direct transition. The band gap can then be obtained by plotting $(\alpha h\nu)^2$ versus $h\nu$ and by extrapolating the linear portion of the absorption edge to find the intercept with energy axis. The dependence of optical band gap on oxygen partial pressure are shown in Fig. 6, the optical band gap of $Zn_{0.93}Mn_{0.07}O$ films was calculated to be in the range of 3.26–3.36 eV. Obviously, the values for optical band gap of $Zn_{0.93}Mn_{0.07}O$ films were smaller than that of the bulk ZnO (3.37 eV) due to Mn doping in ZnO. It is interpreted as being due to the spin-exchange interaction between the *sp* band and localized spins of the transition-metal ions [22,23]. The *s–d* and *p–d* exchange interactions give rise to a negative and a positive correction to the conduction-band and the valence-band energies, respectively, and lead to narrowing of the band gap [22]. According to the Burstein–Moss effect [17], the band gap would increase with increasing carrier concentration. However, the band gap obtained for our ZnMnO films does not accurately follow the Burstein–Moss theory. From Fig. 6, it reveals that the optical band gap increases with increasing oxygen partial pressure until R is 0.4 and then decreases under O_2 overpressure. In this work, the band-gap shift can be understood as the net result of two competing: a widening due to the Burstein–Moss effect, and a narrowing due to many-body effects on the conduction and valence bands [24]. The many-body effects that can shrink the band gap originate from electron interaction and impurity scattering. It has been attributed to the merging of an impurity band into the conduction band, thereby shrinking the band gap and compensating the Burstein–Moss effect. When the density of carrier and defects increased to a critical value, the Burstein–Moss effect is balanced by the many-body effects. The analysis of electrical properties shows that higher carrier concentration leads to a higher impurity scattering. Lower or higher oxygen partial pressure would lead to a higher density of carrier and defects above the critical density, which resulted in the shrinking of band gap. This increase of band gap with the increasing oxygen partial pressure in a certain range is probably due to the reduction of defects at the grain boundaries and a decrease of structural disorder in the films. In addition, the small redshift of the band gap indicate a weaker spin-exchange interaction. Moreover, the decrease of lattice strain in the films with oxygen partial pressure might also have contributed to the increase of energy band gap in the present work.

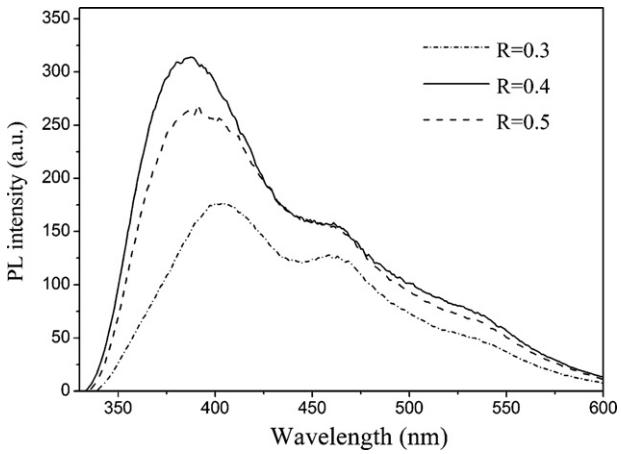

Fig. 7. Room-temperature photoluminescene spectra of $Zn_{0.93}Mn_{0.07}O$ films deposited at different oxygen partial pressures.

3.3.2. Photoluminescence

Fig. 7 shows the room-temperature PL spectra of the films deposited at different oxygen partial pressures. Two emission bands were apparently observed in the PL spectra of $Zn_{0.93}Mn_{0.07}O$ films. One well-resolved PL peak at around 390 nm, together with a broad hump at 450–470 nm, were observed for the $Zn_{0.93}Mn_{0.07}$ thin films. The peak at around 390 nm can be attributed to near-band-edge (NBE) emission in the ZnO host material [25], the other was the visible emission which was commonly associated with the deep-level (DL) emission in $Zn_{0.93}Mn_{0.07}O$ films. Compared with the NBE position of bulk ZnO (3.37 eV), the $Zn_{0.93}Mn_{0.07}O$ films change the position of the NBE band slightly because of the introduction of Mn does not form any donor or acceptor level within the band gap of ZnO (as shown in Fig. 7). This has been discussed in the analysis of electrical properties. The broad humps at around 450–470 nm are related to the blue emission most likely occurs from the donor level of Zn interstitial (Zn_i) to acceptor energy level of Zn vacancy (V_{Zn}) [26]. Generally, the luminescence property of the films has a close relation with the film crystallinity because the density of defects in film reduces with an improvement of the crystallinity. The strong near band emission of the films deposited at a suitable oxygen partial pressure indicates its good quality. From Fig. 7, the intensity of NBE emission is increased with oxygen partial pressure up to 0.4 and then decreased slightly under O_2 overpressure. The FWHM of the peak exhibit same trend that smallest FWHM were shown when R is 0.4. The improved band edge luminescence of the film deposited at certain oxygen partial pressure is attributed to its better overall crystallinity resulting from reduction of strain and defects as well as improvement in crystallite size (both lateral and along growth direction) as observed in XRD and AFM measurements. Zn_i-related emission dramatically decreased with increasing oxygen partial pressure up to R is 0.4. However, Zn_i-related emissions is slightly increased for the $Zn_{0.93}Mn_{0.07}O$ thin film grown under O_2 overpressure. These results demonstrate that the increase of oxygen partial pressure in a certain range leads to the decrease of zinc interstitials and vacancies. Lower or higher oxygen partial pressure would lead to an increase of Zn and oxygen defects, which results in the strengthen DL emission.

The PL results are in line with optical absorption. The strong NBE peak was due to free exciton recombination [27], which was confirmed by the temperature-dependent PL spectra. Considering the exciton binding energy of ZnO (60 meV), the free exciton energy corresponded to the band gap of Mn doped ZnO. It can be seen that the peak position of the emission spectra changes with different oxygen partial pressures. The NBE emission peak position shifts slightly towards the shorter wavelengths with increasing oxygen partial pressure up to 0.4, and then has a red-shift at higher oxygen partial pressures. These were attributed to the optical band gap increases with increasing oxygen partial pressure in a suitable range as indicated by the transmittance studies presented above.

4. Conclusions

In this work, the single-phase $Zn_{1-x}Mn_xO$ films with *c*-axis oriented wurtzite structure were grown on glass substrates by dc reactive magnetron cosputtering. From XRD and XPS measurements, it was confirmed Mn^{2+} substitution for Zn^{2+} lattice sites and Mn concentration was estimated to be approximately 7% for all samples. The experimental results indicated that there was an optimum oxygen partial pressure of R is 0.4 where the film shows relative stronger texture, better nano-crystallite and lower surface roughness. It can be attributed to the reduction of strain and defects as well as improvement in crystallite size. As the oxygen partial pressure increases, the carrier concentration systematically decreases and PL peaks related to zinc interstitials gradually diminish. The minimal resistivity of 70.48 Ω cm with the highest Hall mobility of 1.36 $cm^2 V^{-1} s^{-1}$ and the carrier density of 6.52×10^{16} cm^{-3} were obtained when oxygen partial pressure is 0.4. The optical transmittance and PL spectra of the films are obviously influenced by the oxygen partial pressure. All films exhibit a transmittance higher than 80% in the visible region and a sharp fundamental absorption edge. But the films deposited at $R = 0.4$ showed a lower transmittance than other films. We ascribe it to the lower concentration Zn interstitial atoms. The values for optical band gap of $Zn_{0.93}Mn_{0.07}O$ films were smaller than the bulk ZnO E_g ~3.37 eV due to Mn doping in ZnO. It is interpreted as being due to the spin-exchange interaction between the *sp* band and localized spins of the transition-metal ions. In addition, there is a largest band gap energy of $Zn_{0.93}Mn_{0.07}O$ films deposited at $R = 0.4$ in spite of the lower carrier concentration, which can be ascribed to the weaker many-body effects. PL results show a strong NBE emission and a weak DL emission in all thin films. With the increasing of oxygen partial pressure, the peak of NBE emission has firstly a blueshift to the region of higher photon energy and then redshift, which shows a similar trend to the Eg in the optical transmittance measurement. In conclusion, it is essential to choose the suitable oxygen partial pressure for the purpose to improve the crystallinity and optoelectronic properties of the films.

Acknowledgements

This work was funded by the National Natural Science Foundation of China under Grant No. 60708014, the Natural Science Foundation of Hunan Province under Grant No. 06JJ20034, the Innovation project for postgraduates education of Central South University under Grant No. 062510029, and A Project Supported by Scientific Research Fund of Hunan Provincial Education Department No. 09C321.

References

[1] S.S. Kim, J.H. Moon, B.T. Lee, O.S. Song, J.H. Je, J. Appl. Phys. 95 (2004) 454.
[2] J.K. Furdyna, J. Appl. Phys. 64 (1988) R29.
[3] H. Ohno, Science 281 (1998) 951.
[4] O. Martínez, J.L. Plaza, J. Mass, B. Capote, E. Diéguez, J. Jiménez, Superlattice Microstruct. 42 (2007) 145.
[5] T. Dietl, H. Ohno, F. Matsukura, J. Cibert, D. Ferrand, Science 287 (2000) 1019.
[6] Z.W. Jin, Y.Z. Yoo, T. Sekigushi, T. Chikyoww, H. Ofuchi, H. Fujioka, M. Oshima, H. Koinuma, Appl. Phys. Lett. 83 (2003) 39.
[7] K.J. Kim, Y.R. Park, J. Appl. Phys. 94 (2003) 867.
[8] S.W. Jung, S.J. An, G. Yi, C.U. Jung, S. Lee, S. Cho, Appl. Phys. Lett. 80 (2002) 4561.
[9] U.N. Maiti, P.K. Ghosh, S. Nandy, K.K. Chattopadhyay, Physica B 387 (2007) 103.
[10] L.R.M. Reddy, P. Prathap, K.T.R. Reddy, Curr. Appl. Phys. 9 (2009) 667.
[11] J.M. Li, M.P. dos Santos, Thin Solid Films 250 (1994) 26.
[12] H.Y. Xu, C.S. Xu, Y.C. Liu, C.L. Shao, R. Mu, Appl. Phys. Lett. 88 (2006) 242502.

[13] C. Liu, F. Yun, B. Xiao, S.-J. Cho, Y.T. Moon, H. Morkoç, Morad Abouzaid, R. Ruterana, K.M. Yu, W. Walukiewicz, J. Appl. Phys. 97 (2005) 126107.
[14] M. Chen, Z.L. Pei, C. Sun, L.S. Wen, X. Wang, J. Cryst. Growth 22 (2000) 254.
[15] S.J. Pearton, D.P. Norton, K. Ip, Y.W. Heo, T. Steiner, Prog. Mater. Sci. 50 (2005) 293.
[16] J. Luo, J.K. Liang, Q.L. Liu, F.S. Liu, Y. Zhang, B.J. Sun, G.H. Rao, J. Appl. Phys. 97 (2005) 086106.
[17] H.T. Cao, Z.L. Pei, J. Gong, C. Sun, R.F. Huang, L.S. Wen, Surf. Coat. Technol. 184 (2004) 84.
[18] O. Kappertz, R. Drese, M. Wuttig, J. Vac. Sci. Technol. A: Vac. Surf. Films 20 (2002) 2084.
[19] M. Suchea, S. Christoulakis, N. Katsarakis, T. Kitsopoulos, G. Kiriakidis, Thin Solid Films 515 (2007) 6562.
[20] P. Singh, A.K. Chawla, D. Kaur, R. Chandra, Mater. Lett. 61 (2007) 2050.
[21] S.S. Lin, J.L. Huang, Surf. Coat. Technol. 185 (2004) 222.
[22] Y.R. Lee, A.K. Ramdas, R.L. Aggarwal, Phys. Rev. B 38 (1988) 10600.
[23] R.B. Bylsma, W.M. Becker, J. Kossut, U. Debska, Phys. Rev. B 33 (1986) 8207.
[24] I. Hamberge, C.G. Granqvist, J. Appl. Phys. 60 (1986) R123.
[25] B.X. Lin, Z.X. Fu, Y.B. Jia, Appl. Phys. Lett. 79 (2001) 943.
[26] X.Q. Wei, B.Y. Man, M. Liu, C.S. Xue, H.Z. Zhuang, C. Yang, Physica B 388 (2007) 145.
[27] D.M. Bagnall, Y.F. Chen, Z. Zhu, T. Yao, M.Y. Shen, T. Goto, Appl. Phys. Lett. 73 (1998) 1038.